Article

One-Step Synthesis of Methylene Blue-Encapsulated Zeolitic Imidazolate Framework for Dual-Signal Fluorescent and Homogeneous Electrochemical Biosensing

Jiafu Chang, Wenxin Lv, Qian Li, Haiyin Li, and Feng Li

Anal. Chem., **Just Accepted Manuscript** • DOI: 10.1021/acs.analchem.0c00952 • Publication Date (Web): 01 Jun 2020

One-Step Synthesis of Methylene Blue-Encapsulated Zeolitic Imidazolate Framework for Dual-Signal Fluorescent and Homogeneous Electrochemical Biosensing

Jiafu Chang,[a,b] Wenxin Lv,[a] Qian Li,[a] Haiyin Li,[a,*] and Feng Li[a,b,*]

[a] College of Chemistry and Pharmaceutical Sciences, Qingdao Agricultural University, Qingdao 266109, People's Republic of China

[b] College of Chemistry, Chemical Engineering and Materials Science, Shandong Normal University, Jinan 250014, People's Republic of China

* Corresponding author. Tel/Fax: 86-532-58957855;

E-mail: lifeng@qau.edu.cn (F. Li), lihaiyin@qau.edu.cn (H. Y. Li)

ABSTRACT

In vitro diagnosis requires target biomarkers to be reliably detected at an ultralow level. Dual-signal strategy permits self-calibration to overcome the interferences of experimental and environmental factors, and thus is regarded as a promising approach. However, currently reported works are mainly concentrated on the same forms of energy of output signals. Herein, we propose a one-step strategy for synthesis of methylene blue-encapsulated zeolitic imidazolate framework-90 (MB@ZIF-90) with high loading, unique dual-signal property, exceptional recognitional capability and good stability, and we further pioneer MB@ZIF-90 as a dual-signal biosensor for label-free, enzyme-free, and ultrasensitive detection of adenosine triphosphate (ATP) by integration of fluorescent and homogeneous electrochemical techniques. The recognition of MB@ZIF-90 by target ATP spurs the decomposition of ZIF-90, subsequently permitting MB to be released into supernatant. As compared to the case where ATP doesn't exist, obviously increased intensities in fluorescence and differential pulse voltammetry (DPV) current are observed and both signals are directly proportional to ATP concentrations. Thus, MB@ZIF-90-based biosensor achieved dual-signal detection of ATP in an ultrasensitive manner, and displayed a more reliable diagnosis result than previously reported ATP biosensors. This dual-signal strategy pays a new opportunity to develop high-performance biosensors for in vitro diagnosis, and will demonstrate more application in bioinformatics and clinical medicine.

INTRODUCTION

Biomarker is one of important biochemical indicators, has close concern with the variation in structure and function of organizations, cells and sub cells, and features the higher level of sensibility than imaging and symptom.[1,2] Under this context, development of high-performance biomarker assays is of great meaningful on bioinformatics and clinical medicine, and will provide more important information for various diseases accurate diagnosis.[3,4] However, the expression level of most biomarkers in biological fluids is ultralow and the fluid environments are complex,[5] which are detrimental to efficient and reliable identification of biomarkers. Many techniques including fluorescent,[6-8] electrochemical,[9-11] surface enhanced Raman scattering (SERS),[12-14] and others have been explored for diverse biomarkers sensitive detection based on enzyme-assisted amplification strategy.[15-17] For example, Yuan's group reported an enzyme-assisted cascade catalytic reaction for ultrasensitive electrochemical detection of gene.[18] Nevertheless, no matter what techniques, they detect target objects on the basis of the variation in a single signal. A single signal readout easily leads to inaccuracy due to the affect of nonstandard test administration, different operators and different experimental environments. By contrast, dual signals can obviously improve the diagnosis accuracy due to their self-calibration function, and such a dual-signal strategy has fascinated many people's interests.[19-21] However, the dual signals of reported biosensors belong to the same forms of energy, which inevitably result in a relatively high background noise. It is profitable to construct a dual-signal platform that has different forms of energy and can achieve the output of dual signals in a single assay without addition of other reagents. Whereas, no simple example to develop such a dual-signal biosensor has been proposed, especially for electrochemical and fluorescent signals. Homogeneous electrochemical biosensors, a subclass of electrochemical biosensors, generate different pulse voltammetry (DPV) signals through the diffusion of electroactive dyes toward electrodes without

immobilization of bio-recognizable units, and thus possess the advantages of simplicity, rapidity, sensitivity, and low price, and have attracted a great deal of concern from analytical scientists in the fields of disease diagnosis, food safety, and environment protection.[3,19,22] On the other hand, fluorescence biosensors applied light as an output signal and has more than ~10^3 times increase in sensitivity than colorimetric assays.[23-25] More importantly, the energy form of light is greatly different from that of homogeneous electrochemical biosensor. If homogeneous electrochemical and fluorescent techniques were integrated together, a brand-new dual-signal biosensor for higher-efficiency and more accurate diagnosis of biomarkers will be successfully developed.

Adenosine triphosphate (ATP) is a natural nucleotide consisted of one adenine, one ribose and three phosphate groups, and is a potential biomarker for evaluating cell proliferation and death.[26] When the concentration of ATP turns up abnormal expression in human body, it is broadly regarded to face the risk of angiocardiopathy, parkinsonism, and Alzheimer's diseases.[27-29] In addition, it is reported that the expression level of ATP in brain, serum, and other body fluids is extremely low.[30] Given these information above, substantial efforts have been devoted to development of high-performance ATP biosensors.[31-33] Despite the great progress, it is noteworthy that previous ATP biosensors face the following obstacles. First, most of ATP biosensors devote themselves to a single signal, and the others have dual signals but that belong to the same energy forms. Second, most of ATP biosensors are developed based on aptamer technique, which suffered from strict design of deoxyribonucleic acid (DNA) probes and high-cost/complicated labeling procedure. Third, they required bioenzymes to enhance the detection sensitivity, and thus fail to obtain the rapid response and low-cost test. For settling the problems abovementioned, we strive, here, to develop a label-free, enzyme-free and dual-signal biosensor for ATP ultrasensitive and accurate biosensing by coupling fluorescent and homogeneous electrochemical

techniques.

Zeolitic imidazolate framework-90 (ZIF-90) is a porous and biocompatible metal-organic framework (MOF) built from Zn^{2+} and imidazolate-2-carboxyaldehyde (2-ICA), possesses large surface area and pore size, and is an excellent nanocarrier for encapsulating molecules.[34-36] The procedure for encapsulation generally includes the following steps: first ZIF-90 preparation, second ZIF-90 drying and cleanup of solvent molecules, third loading of molecules in pores, and fourth sealing off the pores, which are complex and costly, result in low loading and poorly controlled release, and produce abundant waste.[37,38] At the same time, the diameters of its pore opening and pore cavity are small, and thus relatively large substances can't be encapsulated inside of ZIF-90.[39] A method to address these obstacles is to introduce ZIF-90 preparation and molecule encapsulation into a one-step operation. Such molecule-encapsulated ZIF-90 composites not only avoid the complicated preparation steps but also increase the loading, enhance the controlled release, and allow the encapsulation of large molecules.[36,40,41] If we introduce a molecule-encapsulated ZIF-90 composite into a ATP biosensor and regulate the loading molecules, such a proposed biosensor would realize the label-free, enzyme-free, ultrasensitive and dual-signal detection of ATP.

Herein, we prepared a methylene blue-encapsulated ZIF-90 (MB@ZIF-90) through combing the fabrication of ZIF-90 and encapsulation of MB in a one-step reaction, in which ZIF-90 and MB were applied as affinity material and signal source, respectively. Experimental measurements demonstrated that MB was effectively encapsulated inside of ZIF-90, and the prepared MB@ZIF-90 possessed high stability under physiological conditions. We further pioneered that MB@ZIF-90 is a promising ATP-responsive dual-signal biosensor due to the competitive coordination between ATP and 2-ICA on Zn^{2+}. Owing to ZIF-90's high loading and unique recognitional capability on ATP, and excellent dual-signal property of

MB, ultrasensitive and dual-signal detection of ATP with label-free and enzyme-free features was realized.

EXPERIMENTAL SECTION

Synthesis of MB@ZIF-90. 4.0 mL N,N-dimethylformamide (DMF) containing 0.0439 g $Zn(CH_3COOH)_2{\cdot}2H_2O$ and 0.0013 g MB was stirred for 15 min. After that, 6.0 mL DMF containing 0.038 g 2-ICA was added, and the final solution reacted for 15 min. Through centrifugation and successive washing with DMF, ultrapure water, and ethanol three times, respectively, MB@ZIF-90 was obtained. For ZIF-90, the preparation process is the same with that of MB@ZIF-90. MB@ZIF-90 was dispersed in HEPES buffer (10 mM, pH 7.4) to get a 10 mg/mL stock solution.

Dual-Signal Detection of ATP Based on MB@ZIF-90. 200 μL of HEPES buffer containing 1.0 mg/mL MB@ZIF-90 and target ATP with different amounts was incubated for 5.0 min. The reaction solution was then centrifugated at 10000 rpm for 1.0 min and the supernatant was exposed to fluorescent and DPV characterizations.

RESULTS AND DISCUSSION

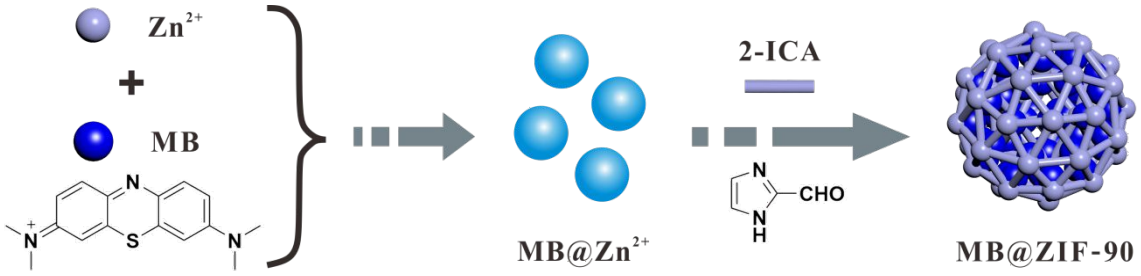

Scheme 1 Schematic diagram of one-step synthesis of MB@ZIF-90.

Synthesis and Characterization of MB@ZIF-90. The illustration for one-step synthesis of MB@ZIF-90 is manifested in Scheme 1. MB has N and S elements that possess weak coordination interaction with metal ions, and thus MB reacts with Zn^{2+} to form coordination intermediate ($MB@Zn^{2+}$). 2-ICA was added to competitively chelate with Zn^{2+} in $MB@Zn^{2+}$ and then ZIF-90 was prepared. Along with the formation of ZIF-90, MB was successfully encapsulated. To validate the formation of

MB@ZIF-90, the identity and phase purity were characterized by X-ray diffraction (XRD) technique (Figure 1A). The peaks of MB@ZIF-90 in the range of 5 º to 40 º were sharp, and were in line with that of prepared ZIF-90 and simulated ZIF-90 single crystal. Besides, there were no unwanted peaks of MB observed. These observations obviously demonstrated that MB@ZIF-90 was of good purity and high crystallinity, and that MB was encapsulated inside of ZIF-90 rather than being physically adsorbed on the surface, and that the encapsulated MB made a minor influence on ZIF-90's lattice distortion. Transmission electron microscopy (TEM) characterization depicted that MB@ZIF-90 exhibited a uniformly dispersed nanospherical morphology (Figure 1B), and their diameter was determined to be 120 nm. To further confirm the loading of MB inside of ZIF-90, Fourier transform infrared spectroscopy (FT-IR) characterizations were carried out (Figure 1C). In comparison with ZIF-90, MB@ZIF-90 displayed new peaks at 1581, 1507, and 576 cm^{-1} that were attributable to MB. Along with the emergence of new FT-IR peaks, the color of MB@ZIF-90 solution changed from white into blue (Figure 1D).

To gain more information about the preparation of MB@ZIF-90 and to disclose MB's dual-signal property, fluorescent and DPV techniques were conducted for MB, ZIF-90, and MB@ZIF-90, respectively (Figure 1E and F). For ZIF-90 and MB@ZIF-90, DPV characterizations were performed by dropping them on indium tin oxide (ITO) electrode to prepare ZIF-90/ITO and MB@ZIF-90/ITO electrodes, respectively. The others were carried out in a homogeneous solution. It is important to note that MB emitted strong fluorescence at 683 nm under the excitation of 610 nm light, and displayed a significant oxidation peak at -0.23 V. Supporting this notion, MB is a good dual-signal source and enables us to achieve the dual-signal fluorescent and homogeneous electrochemical detection of ATP in a single assay. By contrast, FL intensity at 683 nm and peak current at -0.23 V of ZIF-90 are extremely low. It came as no surprise that there is no MB existing inside of ZIF-90 and the signal intensities are dependent on the amount of MB. In this context,

MB@ZIF-90 exhibited higher FL intensity and peak current than that of ZIF-90. This information uncovers that MB was surely loaded inside of ZIF-90 and has unprecedented dual-signal property.

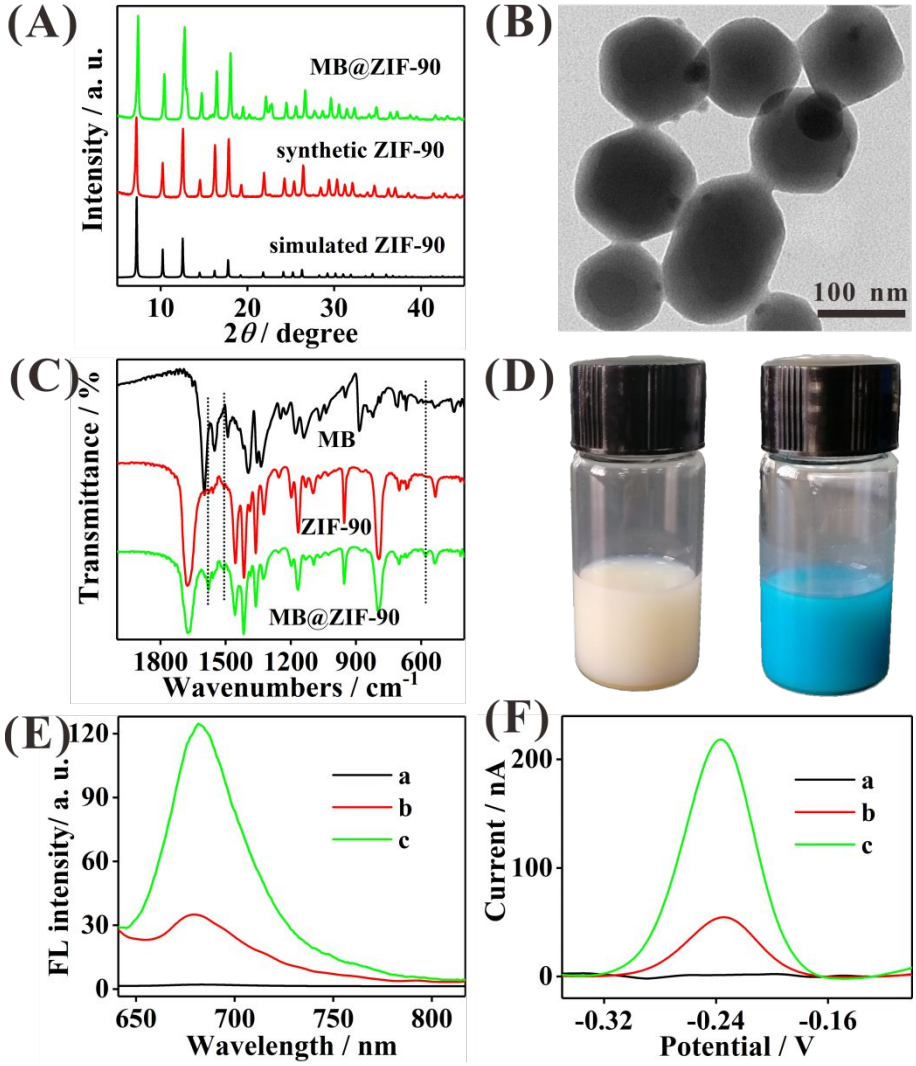

Figure 1 (A) XRD patterns of simulated ZIF-90, synthetic ZIF-90, and MB@ZIF-90. (B) TEM image of MB@ZIF-90. (C) FT-IR spectra of MB, ZIF-90, and MB@ZIF-90. (D) Images of ZIF-90 (left) and MB@ZIF-90 (right) dispersed in water solution. Fluorescence spectra (E) and DPV curves (F) of ZIF-90 (a), MB@ZIF-90 (b) and MB (c).

In view of the affect of stability on diagnosis result, we challenged MB@ZIF-90 by placing it in a reaction buffer containing glucose, bovine serum albumin (BSA), histidine, and dopamine, and a 10-fold diluted serum sample, respectively, and the supernatants obtained through centrifugation were

characterized by fluorescent and DPV techniques. As illustrated in Figure S1A, whether FL intensity or peak current, they all maintained slight change even if the incubation time increased to 36 h, and thus MB@ZIF-90 was stable. Expectedly, no changes in TEM image (Figure S1B) and XRD pattern (Figure S1C) were observed compared with that of untreated MB@ZIF-90. Moreover, FL intensity and peak current are also very low when MB@ZIF-90 existed in serum sample, justifying its sufficient stability for practical application (Figure S1D). Further, MB@ZIF-90 was dispersed into different pH solution for 36 h to assess its response on pH value (Figure S2). Both fluorescent and electrochemical signals were low in the pH range of 4.0 to 11, which implied no leakage of MB, suggesting high pH stability. When pH value was larger than 11 or smaller than 4.0, FL intensity and peak current elevated abruptly, indicating the release of MB and MB@ZIF-90's weak stability in strong acid and base solutions. Meanwhile, the released MB made us be once more sure that MB was effectively loaded inside of ZIF-90.

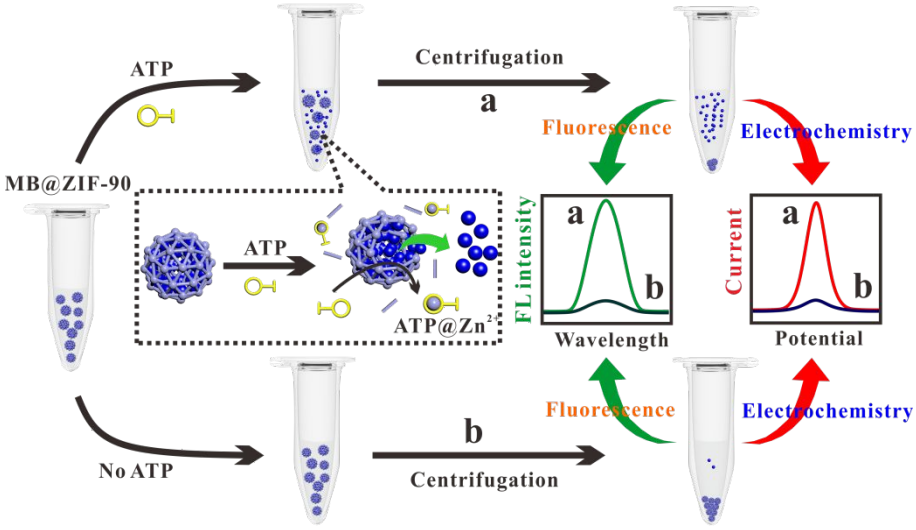

Scheme 2 Schematic representation of MB@ZIF-90-based biosensor for ultrasensitive and dual-signal detection of ATP.

Sensing Principle of MB@ZIF-90-Based Biosensor. Given the abovementioned characteristics, we deduced that MB@ZIF-90 was competent for label-free, enzyme-free and dual-signal detection of ATP in an ultrahigh-sensitivity manner, and the detailed principle was illustrated in Scheme 2.

When ATP was absent, MB@ZIF-90 maintained its structure and morphology minor variation, and the unspoiled ZIF-90 prohibited the release of MB. As a result, no or only small MB was observed in the supernatant, and the detected fluorescent and DPV signals were very low. Whereas, upon the addition of ATP, it decomposed ZIF-90 due to the fact that phosphate group and adenosine group in ATP have stronger coordination with Zn^{2+} than iminazole group in 2-ICA,[36] subsequently leading to the collapse of the ZIF-90 framework and permitting the release of MB from ZIF-90 into solution. Thus, a large diversity of MB was determined in supernatant, and contributed to both high FL intensity and DPV current due to its unique dual-signal property. Considering both the increased signals, MB@ZIF-90-based dual-signal biosensor for label-free, enzyme-free and ultrasensitive detection of ATP was developed based on the integration of fluorescent and homogeneous electrochemical techniques.

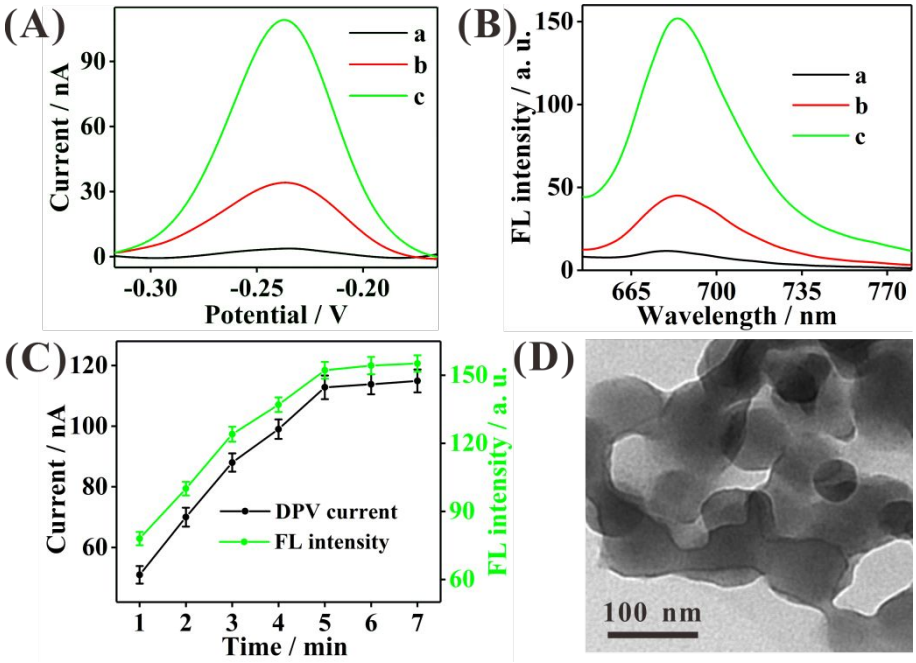

Figure 2 DPV (A) and fluorescent (B) curves of supernatant in the presence of ATP with different amounts: (a) 0, (b) 20 nM, (c) 100 nM. (C) FL intensity and DPV current versus reaction time between MB@ZIF-90 and ATP. (D) TEM image of MB@ZIF-90 after the reaction with 100 nM ATP for 2 min.

Assay Feasibility of MB@ZIF-90-Based Biosensor. To investigate the feasibility of

MB@ZIF-90-based biosensor for ATP assay, reaction solutions that have or don't have ATP were exposed to fluorescence and DPV measurements (Figure 2A and B). If ATP was absent, FL intensity and DPV current of MB were only 12.02 a.u. and 4.13 nA, respectively. Nevertheless, upon the addition of ATP, the supernatant displayed significantly increased fluorescent and electrochemical signals up to 45.00 a.u. and 34.00 nA, respectively. It might be attributable to the fact that large-scale MB were released into supernatant upon the selective decomposition of ZIF-90 by ATP, thereby leading to enhancement in FL intensity and DPV current. Moreover, both signals further increased along with the increasing amount of ATP, demonstrating a definite positive relationship between signal intensity and ATP concentration. This is because more ATP disassemble more ZIF-90 to release more MB into supernatant. Meanwhile, the responsive time only requires 5 min (Figure 2C), to our best knowledge, which is the shortest time to complete the detection of ATP. Both increased signals obviously suggested that label-free, enzyme-free, ultrasensitive and dual-signal detection of ATP could be readily realized using MB@ZIF-90-based biosensor.

Further, UV-vis and TEM techniques were successively employed to characterize the release of MB and the collapse of MB@ZIF-90. The UV-vis curves in Figure S3 demonstrated that the supernatant in the presence of ATP possessed two new peaks at 612 nm and 663 nm (that were assigned to MB) compared with that in the absence of ATP, validating the ATP-initiated efficient release of MB from MB@ZIF-90 too. Besides, after the addition of 100 nM ATP for 2.0 min, MB@ZIF-90 demonstrated an irregular aggregation morphology rather than homogeneous nanospheres (Figure 2D), which might be understood in the terms of the fact that ATP has stronger coordination with Zn^{2+} than 2-ICA, further damaging ZIF-90 accompanied by the release of MB.

To investigate such an ATP-responsive fluorescence and DPV current turn-on phenomenon,

competitive interaction between ATP and 2-ICA on Zn^{2+} was examined. The experiment was proposed by pre-reaction of ATP and adenosine triphosphatase (ATPase), and subsequent addition of MB@ZIF-90 (Figure S4A). ATPase catalyzed hydrolysis of ATP into adenosine diphosphate (ADP), which doesn't have the stronger coordination interaction with Zn^{2+} than 2-ICA, leading to no release of MB. Therefore, FL intensity and DPV current of MB in supernatant were very low. As illustrated in Figure S4B, in comparison with the case that ATPase didn't exist, the pre-reaction of ATPase with ATP resulted in both low fluorescent and electrochemical signals that are about identical with that of individual MB@ZIF-90, obtained from the high catalyzing efficiency of ATPase toward ATP and subsequent vanishment of ATP-initiated the collapse of MB@ZIF-90.

Analytical Performance of MB@ZIF-90-Based Biosensor. To evaluate the sensing ability of MB@ZIF-90-based biosensor for ultrasensitive and dual-signal detection of ATP, an array of solutions containing ATP with different concentrations were exposed to fluorescent and electrochemical measurements. As depicted in Figure 3A and C, the fluorescence and current responses of MB elevated along with the raising of ATP concentrations, displaying a directly positive relationship between signal intensity and ATP amounts. Calibration plots were further obtained through applying FL intensity (F) and peak current (I) as vertical coordinates, and ATP concentrations (C_{ATP}) from 1 to 100 nM and 0.1 to 100 nM as horizontal coordinates, respectively. They demonstrated a high linearity with coefficients of 0.9950 and 0.9919 (Figure 3B and D), and the equations were determined to be $F = 1.28C_{ATP} + 23.205$ and $I = 1.0275C_{ATP} + 10.4905$. The detection limits reached 0.38 nM for fluorescent technique and 0.027 nM for homogeneous electrochemical technique based on 3σ, respectively, and were compared with that of other methods in Table S1. Obviously, the detection limit was comparable to or smaller than those of previously reported probes that focused on single-signal determination of ATP based on aptamer strategy, being

governed by complex and high-cost labeling process, strict design of DNA sequences and expensive bioenzymes. This high performance may result from ZIF-90's porous structure and one-step preparation strategy enabling the encapsulation of a large diversity of MB, and exceptional recognitional capability of ZIF-90 on ATP permitting for a significant raise in the concentration of released MB upon the addition of only a handful of ATP. Overall, this MB@ZIF-90-based biosensor possessed apparent merits of simple operation, fast analysis, and low price, and therefore was regarded as a more popular tool for ultrasensitive and dual-signal analysis of ATP, favoring the rapid, early and accurate diagnosis of ATP-related diseases.

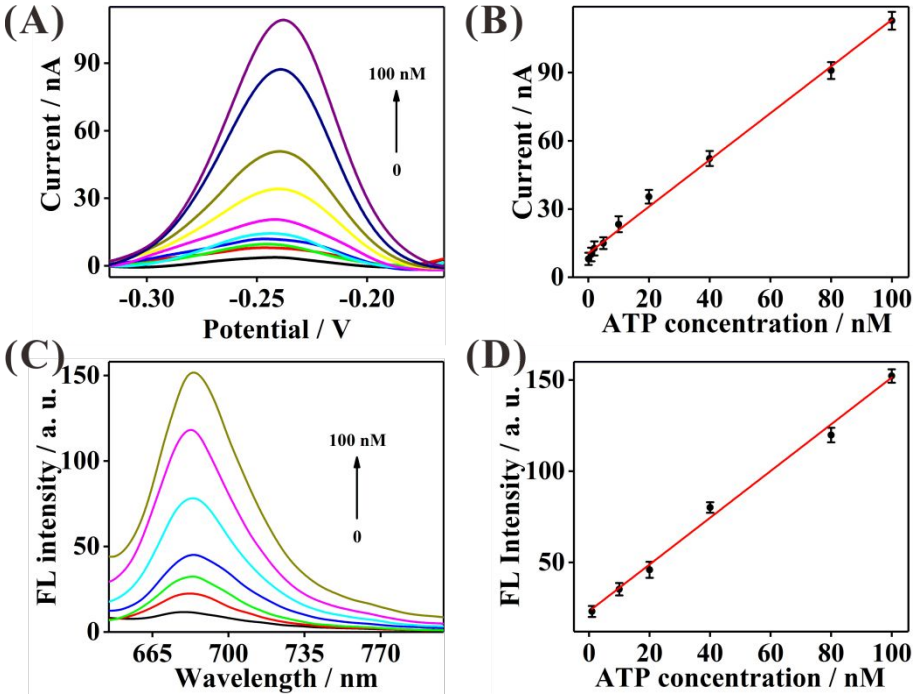

Figure 3 (A) DPV responses of supernatant upon the addition of ATP with different concentrations: 0, 0.1, 1, 2, 5, 10, 20, 40, 80, 100 nM. (B) Linear relationship between current and ATP concentration. (C) Fluorescence spectra of supernatant upon the addition of ATP with different concentrations: 0, 1, 10, 20, 40, 80, 100 nM. (D) Linear relationship between FL intensity and ATP concentration.

Selectivity, Stability, and Precision. ADP, adenosine monophosphate (AMP) and pyrophosphate (PPi) that have similar structure with ATP, and glucose, BSA, histidine and dopamine that may co-exist with ATP in biological samples, were applied as interfering molecules to examine the selectivity and

anti-interference ability of MB@ZIF-90-based biosensor (Figure 4A). The ΔI ($\Delta I = I_{ATP} - I_0$, where I_{ATP} is the current of supernatant in the presence of ATP, and I_0 is the current of supernatant in the absence of ATP) and ΔF ($\Delta F = F_{ATP} - F_0$, where F_{ATP} is the FL intensity of supernatant in the presence of ATP, and F_0 is the FL intensity of supernatant in the absence of ATP) of ATP was 3.6 and 4.24, 4.5 and 4.82, 3.27 and 3.88, 18.21 and 15.5, 21.62 and 17.5, 15.43 and 14.35, and 16.61 and 14.73 times higher than that of ADP, AMP, PPi, glucose, BSA, histidine, and dopamine, respectively. Furthermore, it was revealed that the variations in FL intensity and DPV current of MB in the presence of ATP and the interferences were only 17.6 a.u. and 8.6 nA compared with that in the presence of ATP alone, undoubtedly implying that MB@ZIF-90-based biosensor had distinguished specificity for discriminating ATP against other matters, especially ADP and AMP, and strong anti-interference ability. The stability of this biosensor was tested by keeping MB@ZIF-90 in a dark environment at 4 °C for 36 h, and subsequently this sensor was employed to detect 100 nM ATP. Both detected fluorescent and electrochemical signals maintained 103.7% and 105.1% of that gotten from untreated MB@ZIF-90, justifying the high stability (Figure S5A). Further, the inter-assay precision of the proposed biosensor was studied through employing six differently prepared MB@ZIF-90 in the analysis of 100 nM ATP (Figure S5B). The calculated relative standard deviations (RSDs) were around 4.3% and 3.7% for fluorescent and electrochemical techniques, respectively, indicating an acceptable fabrication repeatability.

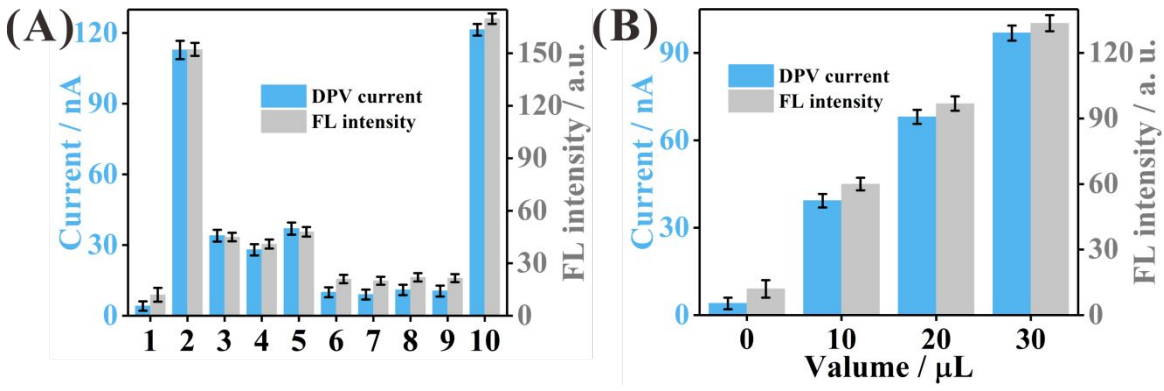

Figure 4 (A) Selectivity experiment of MB@ZIF-90-based biosensor for ATP: (1) blank, (2) ATP, (3) ADP, (4) AMP, (5) PPi, (6) glucose, (7) histidine, (8) dopamine, (9) BSA, (10) mixture. (B) FL intensity and DPV current of MB@ZIF-90-based biosensor corresponding to different volumes of MCF cell lysis solution: 0, 10, 20, 30 μL. The total detection volume was 200 μL.

Real Sample Analysis. To test the applicability of MB@ZIF-90-based biosensor for ATP in clinical sample, recovery experiments were first conducted by spiking ATP with different amounts into diluted human serum samples (Table S2). The recoveries were calculated to be 102.1 % (101.7 %), 102.15 % (98.95 %), and 101.36 % (102.24 %) for the assay of 10, 20, and 50 nM ATP, and the RSDs were around 3.32 % (3.25 %), 3.62 % (3.17 %), and 2.93 % (3.37 %), respectively. The acceptable recoveries and low RSDs suggested the good reproducibility. Further, MB@ZIF-90-based biosensor was employed to detect ATP in MCF-7 cell lysis solution at a density of 1.0×10^6 cells/mL. The MCF-7 cell lysis solution was diluted with a HEPES buffer before analyzing. It can be clearly seen from Figure 4B that with the volume of lysis solution increasing, the resultant solution displayed a gradually increased fluorescent and DPV signals. Through the change in FL intensity and DPV current, the expression level of ATP in MCF-7 cell lysis solution was determined to be 5.63 mM for fluorescent technique and 5.75 mM for homogeneous electrochemical technique, which were in good agreement with that of previously reported methods.[42]

CONCLUSIONS

In summary, we have proposed a one-step strategy for preparation of MB-encapsulated ZIF-90 (MB@ZIF-90) with high loading, unique dual-signal property, and splendid stability, and we have also displayed its application in development of label-free, enzyme-free, ultrasensitive, and dual-signal biosensor, using ATP as the proof-of-concept analyte. Compared with previously reported ATP biosensors, MB@ZIF-90-based biosensor had several advantages as follows. First, this is the first example to develop

dual-signal biosensor for ATP assay with different energy forms. Second, it fully utilizes the high loading of ZIF-90 toward MB and exceptional recognitional capability of ZIF-90 on ATP to achieve ATP biosensing with low detection limit and shortest detection time. Third, it abandons DNA probes and bioenzymes and possesses the advantages of simple operation and low cost. Moreover, the promising strategy is also applicable to other functional molecules and opens up a new path to develop dual-signal biosensors, thus providing a promising approach for ATP-related diseases more accurate diagnosis.

Notes

The authors declare no competing financial interest.

ACKNOWLEDGEMENTS

This work was financially supported by National Natural Science Foundation of China (21605093 and 21775082), the Shandong Province Higher Educational Program for Young Innovation Talents, the Major Program of Shandong Province Natural Science Foundation (ZR2018ZC0127), and the Special Foundation for Distinguished Taishan Scholar of Shandong Province (ts201511052).

SUPPORTING INFORMATION

Additional information as noted in the text. Table S1and S2, and Figure S1-S5 as described in the text.

REFERENCES

(1) Sawyers, C. L. The Cancer Biomarker Problem. *Nature* **2008**, *452*, 548–552.

(2) Sapra, R.; Verma, R. P.; Maurya, G. P.; Dhawan, S.; Babu, J.; Haridas, V. Designer Peptide and Protein Dendrimers: A Cross-Sectional Analysis. *Chem. Rev.* **2019**, *119*, 11391–11441.

(3) Chang, J. F.; Wang, X.; Wang, J.; Li, H. Y.; Li, F. Nucleic Acid-Functionalized Metal–Organic Framework-Based Homogeneous Electrochemical Biosensor for Simultaneous Detection of Multiple Tumor Biomarkers. *Anal. Chem.* **2019**, *91*, 3604–3610.

(4) Bock, C.; Halbritter, F.; Carmona, F. J.; Tierling, S.; Datlinger, P.; Assenov, Y.; Berdasco, M.; Bergmann, A. K.; Booher, K.; Busato, F.; Campan, M.; Dahl, C.; Dahmcke, C. M.; Diep, D.; Fernández, A. F.; Gerhauser, C.; Haake, A.; Heilmann, K.; Holcomb, T.; Hussmann, D., et al. Quantitative Comparison of DNA Methylation Assays for Biomarker Development and Clinical Applications. *Nat. Biotechnol.* **2016**, *34*, 726–737.

(5) Shi, J.; Deng, Q. C.; Wan, C. Y.; Zheng, M. M.; Huang, F. H.; Tang, B. Fluorometric Probing of the Lipase Level as Acute Pancreatitis Biomarkers based on Interfacially Controlled Aggregation-Induced Emission (AIE). *Chem. Sci.* **2017**, *8*, 6188–6195.

(6) Li, P. X.; Wei, M.; Zhang, F.; Su, J.; Wei, W.; Zhang, Y. J.; Liu, S. Q. Novel Fluorescence Switch for MicroRNA Imaging in Living Cells Based on DNAzyme Amplification Strategy. *ACS Appl. Mater. Interfaces* **2018**, *10*, 43405–43410.

(7) Tang, X.; Deng, R. J.; Sun, Y. P.; Ren, X. J.; Zhou, M. X.; Li, J. H. Amplified Tandem Spinach-Based Aptamer Transcription Enables Low Background miRNA Detection. *Anal. Chem.* **2018**, *90*, 10001–10008.

(8) Miao, X. M.; Cheng, Z. Y.; Ma, H. Y.; Li, Z. B.; Xue, N.; Wang, P. Label-Free Platform for MicroRNA Detection Based on the Fluorescence Quenching of Positively Charged Gold Nanoparticles to Silver Nanoclusters. *Anal. Chem.* **2018**, *90*, 1098–1103.

(9) Koo, K. M.; Carrascosa, L. G.; Trau, M. DNA-directed Assembly of Copper Nanoblocks with Inbuilt Fluorescent and Electrochemical Properties: Application in Simultaneous Amplification-Free Analysis of Multiple RNA Species. *Nano Res.* **2018**, *11*, 940–952.

(10) Deng, L.; Wu, Y. H.; Xu, S. X.; Tang, Y. R.; Zhang, X. F.; Wu, P. Improving the Signal-to-Background Ratio during Catalytic Hairpin Assembly through Both-End-Blocked DNAzyme. *ACS Sensors* **2018**, *3*, 1190–1195.

(11) Qin, X. L.; Dong, Y. F.; Wang, M. H.; Zhu, Z. W.; Li, M. X.; Chen, X. J.; Yang, D.; Shao, Y. H. C-dots Assisted Synthesis of Gold Nanoparticles as Labels to Catalyze Copper Deposition for Ultrasensitive Electrochemical Sensing of Proteins. *Sci. China Chem.* **2018**, *61*, 476–482.

(12) Lenzi, E.; Jimenez de Aberasturi, D.; Liz-Marzán, L. M. Surface-Enhanced Raman Scattering Tags for Three-Dimensional Bioimaging and Biomarker Detection. *ACS Sensors* **2019**, *4*, 1126–1137.

(13) Saleh, T. A.; Al-Shalalfeh, M. M.; Al-Saadi, A. A. Silver Loaded Graphene as a Substrate for Sensing 2-Thiouracil using Surface-Enhanced Raman Scattering. *Sens. Actuators B: Chem.* **2018**, *254*, 1110–1117.

(14) Lee, T.; Wi, J.-S.; Oh, A.; Na, H.-K.; Lee, J.; Lee, K.; Lee, T. G.; Haam, S. Highly Robust, Uniform and Ultra-Sensitive Surface-Enhanced Raman Scattering Substrates for microRNA Detection Fabricated by using Silver Nanostructures Grown in Gold Nanobowls. *Nanoscale* **2018**, *10*, 3680-3687.

(15) Wang, M. H.; Yin, H. S.; Zhou, Y. L.; Meng, X. J.; Waterhouse, G. I. N.; Ai, S. Y. A Novel Photoelectrochemical Biosensor for the Sensitive Detection of Dual microRNAs Using Molybdenum Carbide Nanotubes as Nanocarriers and Energy Transfer between CQDs and AuNPs. *Chem. Eng. J.* **2019**, *365*, 351–357.

(16) Qiu, Z.; Shu, J.; Tang, D. P. Near-Infrared-to-Ultraviolet Light-Mediated Photoelectrochemical Aptasensing Platform for Cancer Biomarker Based on Core–Shell NaYF4:Yb,Tm@TiO_2 Upconversion Microrods. *Anal. Chem.* **2018**, *90*, 1021–1028.

(17) Rashidiani, J.; Kamali, M.; Sedighian, H.; Akbariqomi, M.; Mansouri, M.; Kooshki, H. Ultrahigh Sensitive Enhanced-Electrochemiluminescence Detection of Cancer Biomarkers using Silica NPs/Graphene Oxide: A Comparative Study. *Biosens. Bioelectron.* **2018**, *102*, 226–233.

(18) Wang, D.; Chai, Y. Q.; Yuan, Y. L.; Yuan, R. Precise Regulation of Enzyme Cascade Catalytic Efficiency with DNA Tetrahedron as Scaffold for Ultrasensitive Electrochemical Detection of DNA. *Anal. Chem.* **2019**, *91*, 3561–3566.

(19) Chang, J. F.; Li, H. Y.; Li, F. Diffusivity and Intercalation of Electroactive Dyes-Mediated Truly Ratiometric Homogeneous Electrochemical Strategy for Highly Sensitive Biosensing. *Chem. Commun.* **2019**, *55*, 10603–10606.

(20) Wang, H.; Pu, G. Q.; Devaramani, S.; Wang, Y. F.; Yang, Z. F.; Li, L. F.; Ma, X. F.; Lu, X. Q. Bimodal Electrochemiluminescence of G-CNQDs in the Presence of Double Coreactants for Ascorbic Acid Detection. *Anal. Chem.* **2018**, *90*, 4871–4877.

(21) Cai, X.-L.; Zheng, B.; Zhou, Y.; Younis, M. R.; Wang, F.-B.; Zhang, W.-M.; Zhou, Y.-G.; Xia, X.-H.

Synergistically Mediated Enhancement of Cathodic and Anodic Electrochemiluminescence of Graphene Quantum Dots through Chemical and Electrochemical Reactions of Coreactants. *Chem. Sci.* **2018**, *9*, 6080–6084.

(22) Fu, C. L.; Liu, C.; Li, Y.; Guo, Y. J.; Luo, F.; Wang, P. L.; Guo, L. H.; Qiu, B.; Lin, Z. Y. Homogeneous Electrochemical Biosensor for Melamine Based on DNA Triplex Structure and Exonuclease III-Assisted Recycling Amplification. *Anal. Chem.* **2016**, *88*, 10176–10182.

(23) Greenwald, E. C.; Mehta, S.; Zhang, J. Genetically Encoded Fluorescent Biosensors Illuminate the Spatiotemporal Regulation of Signaling Networks. *Chem. Rev.* **2018**, *118*, 11707–11794.

(24) Lau, D.; Walsh, J. C.; Peng, W.; Shah, V. B.; Turville, S.; Jacques, D. A.; Böcking, T. Fluorescence Biosensor for Real-Time Interaction Dynamics of Host Proteins with HIV-1 Capsid Tubes. *ACS Appl. Mater. Interfaces* **2019**, *11*, 34586–34594.

(25) Capilli, G.; Cavalera, S.; Anfossi, L.; Giovannoli, C.; Minella, M.; Baggiani, C.; Minero, C. Amine-Rich Carbon Nitride Nanoparticles: Synthesis, Covalent Functionalization with Proteins and Application in a Fluorescence Quenching Assay. *Nano Res.* **2019**, *12*, 1862–1870.

(26) Liu, Z. C.; Wu, P. C.; Yin, Y. Y.; Tian, Y. A Ratiometric Fluorescent DNA Nanoprobe for Cerebral Adenosine Triphosphate Assay. *Chem. Commun.* **2019**, *55*, 9955–9958.

(27) Li, S.; Zhao, X. T.; Yu, X. X.; Wan, Y. Q.; Yin, M. Y.; Zhang, W. W.; Cao, B. Q.; Wang, H. Fe_3O_4 Nanozymes with Aptamer-Tuned Catalysis for Selective Colorimetric Analysis of ATP in Blood. *Anal. Chem.* **2019**, *91*, 14737–14742.

(28) Li, X.; Yang, J. M.; Xie, J. Q.; Jiang, B. Y.; Yuan, R.; Xiang, Y. Cascaded Signal Amplification via Target-Triggered Formation of Aptazyme for Sensitive Electrochemical Detection of ATP. *Biosens. Bioelectron.* **2018**, *102*, 296–300.

(29) Tan, K.-Y.; Li, C.-Y.; Li, Y.-F.; Fei, J. J.; Yang, B.; Fu, Y.-J.; Li, F. Real-Time Monitoring ATP in Mitochondrion of Living Cells: A Specific Fluorescent Probe for ATP by Dual Recognition Sites. *Anal. Chem.* **2017**, *89*, 1749–1756.

(30) Zhang, K. L.; He, X. L.; Liu, Y.; Yu, P.; Fei, J. J.; Mao, L. Q. Highly Selective Cerebral ATP Assay Based on Micrometer Scale Ion Current Rectification at Polyimidazolium-Modified Micropipettes. *Anal. Chem.* **2017**, *89*, 6794–6799.

(31) Lu, L.; Si, J. C.; Gao, Z. F.; Zhang, Y.; Lei, J. L.; Luo, H. Q.; Li, N. B. Highly Selective and Sensitive Electrochemical Biosensor for ATP Based on the Dual Strategy Integrating the Cofactor-Dependent

Enzymatic Ligation Reaction with Self-Cleaving DNAzyme-Amplified Electrochemical Detection. *Biosens. Bioelectron.* **2015**, *63*, 14–20.

(32) Fan, Y.-Y.; Mou, Z.-L.; Wang, M.; Li, J.; Zhang, J.; Dang, F.-Q.; Zhang, Z.-Q. Chimeric Aptamers-Based and MoS_2 Nanosheet-Enhanced Label-Free Fluorescence Polarization Strategy for Adenosine Triphosphate Detection. *Anal. Chem.* **2018**, *90*, 13708–13713.

(33) Xu, Y. Y.; Xu, J.; Xiang, Y.; Yuan, R.; Chai, Y. Q. Target-Induced Structure Switching of Hairpin Aptamers for Label-Free and Sensitive Fluorescent Detection of ATP via Exonuclease-Catalyzed Target Recycling Amplification. *Biosens. Bioelectron.* **2014**, *51*, 293–296.

(34) Morris, W.; Doonan, C. J.; Furukawa, H.; Banerjee, R.; Yaghi, O. M. Crystals as Molecules: Postsynthesis Covalent Functionalization of Zeolitic Imidazolate Frameworks. *J. Am. Chem. Soc.* **2008**, *130*, 12626–12627.

(35) Brown, A. J.; Johnson, J. R.; Lydon, M. E.; Koros, W. J.; Jones, C. W.; Nair, S. Continuous Polycrystalline Zeolitic Imidazolate Framework-90 Membranes on Polymeric Hollow Fibers. *Angew. Chem., Int. Ed.* **2012**, *51*, 10615–10618.

(36) Deng, J. J.; Wang, K.; Wang, M.; Yu, P.; Mao, L. Q. Mitochondria Targeted Nanoscale Zeolitic Imidazole Framework-90 for ATP Imaging in Live Cells. *J. Am. Chem. Soc.* **2017**, *139*, 5877–5882.

(37) Kahn, J. S.; Freage, L.; Enkin, N.; Garcia, M. A. A.; Willner, I. Stimuli-Responsive DNA-Functionalized Metal–Organic Frameworks (MOFs). *Adv. Mater.* **2017**, *29*, 1602782.

(38) Wu, S.; Li, C.; Shi, H.; Huang, Y.; Li, G. X. Design of Metal–Organic Framework-Based Nanoprobes for Multicolor Detection of DNA Targets with Improved Sensitivity. *Anal. Chem.* **2018**, *90*, 9929–9935.

(39) Zheng, H. Q.; Zhang, Y. N.; Liu, L. F.; Wan, W.; Guo, P.; Nyström, A. M.; Zou, X. D. One-Pot Synthesis of Metal–Organic Frameworks with Encapsulated Target Molecules and Their Applications for Controlled Drug Delivery. *J. Am. Chem. Soc.* **2016**, *138*, 962–968.

(40) Alsaiari, S. K.; Patil, S.; Alyami, M.; Alamoudi, K. O.; Aleisa, F. A.; Merzaban, J. S.; Li, M.; Khashab, N. M. Endosomal Escape and Delivery of CRISPR/Cas9 Genome Editing Machinery Enabled by Nanoscale Zeolitic Imidazolate Framework. *J. Am. Chem. Soc.* **2018**, *140*, 143–146.

(41) Chen, T.-T.; Yi, J.-T.; Zhao, Y.-Y.; Chu, X. Biomineralized Metal–Organic Framework Nanoparticles Enable Intracellular Delivery and Endo-Lysosomal Release of Native Active Proteins. *J. Am. Chem. Soc.* **2018**, *140*, 9912–9920.

(42) Xu, X.; Nan, D. Y.; Yang, H.; Pan, S.; Liu, H.; Hu, X. L. Quercetin@ZIF-90 as a Novel Antioxidant

for Label-free Colorimetric ATP Sensing at Neutral pH. *Sens. Actuators B: Chem.* **2020**, *304*, 127324.

For TOC only

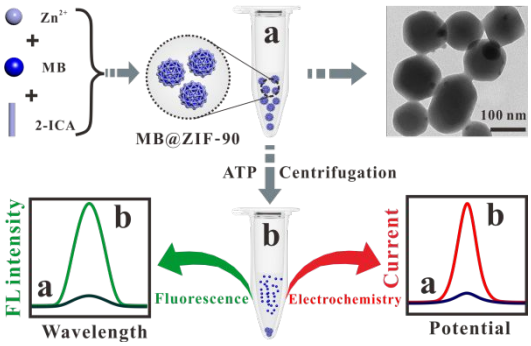
Zn2+
MB
2-ICA
MB@ZIF-90
a
100 nm
ATP
Centrifugation
b
FL intensity
a
b
Wavelength
Fluorescence
Electrochemistry
Current
a
b
Potential